Straining and Attachment of Colloids in Physically Heterogeneous Porous Media

Scott A. Bradford,* Mehdi Bettahar, Jirka Simunek, and Martinus Th. van Genuchten

ABSTRACT

Colloid transport studies were conducted in water-saturated physically heterogeneous systems to gain insight into the processes controlling transport in natural aquifer and vadose zone (variably saturated) systems. Stable monodispersed colloids (carboxyl latex microspheres) and porous media (Ottawa quartz sands) that are negatively charged were employed in these studies. The physically heterogeneous systems consisted of various combinations of a cylindrical sand lens embedded in the center of a larger cylinder of matrix sand. Colloid migration was found to strongly depend on colloid size and physical heterogeneity. A decrease in the peak effluent concentration and an increase in the colloid mass removal in the sand near the column inlet occurred when the median grain size of the matrix sand decreased or the size of the colloid increased. These observations and numerical modeling of the transport data indicated that straining was sometimes an important mechanism of colloid retention. Experimental and simulation results suggest that attachment was more important when the colloid size was small relative to the sand pore size. Transport differences between conservative tracers and colloids were attributed to flow bypassing of finer-textured sands, colloid retention at interfaces of soil textural contrasts, and exclusion of colloids from smaller pore spaces. Colloid retention in the heterogeneous systems was also influenced by spatial variations in the pore water velocity. Parameters in straining and attachment models were successfully optimized to the colloid transport data. The straining model typically provided a better description of the effluent and retention data than the attachment model, especially for larger colloids and finer-textured sands. Consistent with previously reported findings, straining occurred when the ratio of the colloid and median grain diameters was >0.5%.

INORGANIC, ORGANIC, and microbiological colloids exist in natural and contaminated aquifer and vadose zone environments. These colloid particles can be released into soil solution and groundwater through a variety of hydrologic, geochemical, and microbiological processes (MacCarthy and Zachara, 1989; Ryan and Elimelech, 1996). Knowledge of the processes that control colloid transport and fate is required to assess the contamination potential and to protect drinking water supplies from pathogenic microorganisms (Bitton and Harvey, 1992), to develop engineered bioaugmentation and bioremediation strategies (Wilson et al., 1986), and to devise microbially enhanced oil recovery systems (MacLeod et al., 1988). Furthermore, the high surface area of colloids facilitates the sorption of many organic and inorganic contaminants. Colloids can then act as a mobile solid phase that accelerates the transport of sorbed contaminants (Kretzschmar et al., 1999; Ouyang et al., 1996).

Many soil column and batch experiments have been conducted to quantify fundamental properties and processes that control colloid transport and fate in the subsurface, including sedimentation (Wan et al., 1995), hydrodynamics (Wang et al., 1981; Tan et al., 1994), ionic strength (Abu-Sharar et al., 1987), pH (Suarez et al., 1984), chemical heterogeneity (Song and Elimelech, 1994; Song et al., 1994), hydrophobicity (Bales et al., 1993), and surfactants (Ryan and Gschwend, 1994). The primary mechanism of colloid mass removal by the soil is typically ascribed to colloid attachment. Attachment is the removal of colloids from solution via collision with and fixation to the solid phase, and is dependent on colloid–colloid, colloid–solvent, and colloid–porous media interactions. According to traditional clean-bed attachment theory (first-order attachment), colloid removal by a filter bed decreases exponentially with depth. Colloid attachment theory also predicts an optimum particle size for transport for a given aqueous-porous medium system (Yao et al., 1971; Rajagopalan and Tien, 1976). Smaller particles are predicted to be removed more efficiently by diffusive transport, and larger particles by sedimentation and interception.

Experimental observations of colloid transport are not always in agreement with colloid attachment theory (Tufenkji et al., 2003). For example, researchers have reported enhanced colloid retention at the soil surface (Camesano and Logan, 1998) and that the spatial distribution of retained colloids does not follow a simple exponential decrease with depth (Bolster et al., 1999; Redman et al., 2001; Bradford et al., 2002). Some of these discrepancies have been attributed to soil surface roughness (Kretzschmar et al., 1997; Redman et al., 2001), charge heterogeneity (Johnson and Elimelech, 1995), and variability in colloid characteristics (Bolster et al., 1999). A time-dependent attachment rate has also been reported to occur as a result of differences in the attachment behavior of colloids on clean porous media and on media already containing attached colloids (Johnson and Elimelech, 1995). Blocking and ripening refer to decreasing and increasing attachment with time, respectively.

Some of the discrepancies between colloid transport data and attachment theory may also be due to the fact that attachment theory does not account for straining. Straining is the trapping of colloid particles in down-gradient pore throats that are too small to allow particle passage (McDowell-Boyer et al., 1986). The magnitude of colloid retention by straining depends on both colloid and porous medium properties. Straining occurs when colloids are retained in dead-end pores that are smaller than some critical size. Colloid transport may still occur in pores that are larger than this critical size. Sakthivadi-

---

S.A. Bradford, M. Bettahar, J. Simunek, and M.Th. van Genuchten, George E. Brown, Jr. Salinity Laboratory, USDA, ARS, 450 West Big Springs Road, Riverside CA 92507-4617. Received 1 May 2003. Special Section: Colloids and Colloid-Facilitated Transport of Contaminants in Soils. *Corresponding author (sbradford@ussl.ars.usda.gov).

Abbreviations: PV, pore volume.

vel (1966, 1969) and Herzig et al. (1970) developed geometric relations between the effective diameter of colloids and soil grain-size distribution characteristics to predict mass removal by straining. Matthess and Pekdeger (1985) generalized this rule to porous media made up of a distribution of grain sizes. Colloid transport data from Harvey et al. (1993) and Bradford et al. (2002) indicate that straining was more pronounced than predictions based on the criteria given by Matthess and Pekdeger (1985). Harvey et al. (1993) observed a trend of increasing colloid retention with increasing colloid size and hypothesized that this straining behavior was due to migration of clay particles to one end of the column (decreasing the pore size at this location). Bradford et al. (2002) reported that effluent colloid concentration curves and the final spatial distributions of retained colloids by the porous media were highly dependent on the colloid size and soil grain-size distribution. Relative peak effluent concentrations decreased and mass removal of colloids near the column inlet increased when colloid size increased and soil median grain size decreased. These observations were attributed to colloid straining since conventional attachment and blocking models could not describe this behavior. Bradford et al. (2003) employed an irreversible depth-dependent straining coefficient to successfully model straining.

Laboratory-scale studies that explore the role of subsurface heterogeneity on colloid transport are important to bridge the gap in knowledge between field-scale and homogeneous soil column studies. This is especially true for larger-sized colloids, which may undergo size exclusion in heterogeneous systems (Ryan and Elimelech, 1996) as well as straining (Bradford et al., 2002). Relatively few laboratory-scale studies have been conducted to explore the influence of heterogeneity on colloid migration in porous media (Saiers et al., 1994; Silliman, 1995), although laboratory-scale studies have examined the influence of fractures on colloid migration (Reimus, 1995; Cumbie and McKay, 1999). Saiers et al. (1994) measured the transport behavior of colloidal silica (mean colloid diameter of 0.091 μm) in systems composed of a coarse (mean grain size of 870 μm) soil lens embedded in a finer (mean grain size of 360 μm) soil matrix. These authors found that colloid transport and attachment could be adequately described with an advection–dispersion transport model that accounted for first-order kinetic attachment–detachment. Silliman (1995) measured the transport behavior of a distribution of latex microspheres (diameters ranging from 2 to 90 μm) in various configurations of three coarse-textured sands (mean grain diameters equal to 3400, 2030, and 925 μm). Results from this study showed significant colloid retention at media contacts where water moved from larger to smaller diameter sands. Silliman (1995) attributed this observation to attachment leading to increased straining since colloid attachment decreases the effective pore size at a particular location and reversing the direction of water flow liberated large numbers of colloids.

The objective of this work was to investigate processes controlling the transport and fate of colloids in physical heterogeneous subsurface systems. Colloid transport experiments were conducted in physically heterogeneous systems consisting of various combinations of a cylindrical soil lens embedded in the center of a larger cylinder of matrix soil. These studies were performed under saturated conditions, but have implications for the variably saturated vadose zone. Transport and retention was assessed by measuring temporal changes in colloid effluent concentrations and studying the final spatial distribution of colloids remaining in the soil columns. The data were interpreted with the aid of conservative tracer (bromide) studies conducted simultaneously on the same soil columns, and numerical modeling of the experimental systems. Special attention will be given to the role of colloid straining in physical heterogeneous systems.

MATERIALS AND METHODS

Many of the experimental materials, procedures, and protocols employed in this study were used also for homogeneous soil column experiments described by Bradford et al. (2002). Yellow-green fluorescent latex microspheres (Interfacial Dynamics Company, Portland, OR) were used as model colloid particles in the experimental studies (excitation at 490 nm, and emission at 515 nm). Two size diameters of colloid particles (d_p), 1.0 and 3.2 μm, were employed. These microspheres had carboxyl surface functional groups grafted onto latex particle surfaces by the manufacturer to create a negatively charged hydrophobic colloid surface with a particle density of 1.055 g cm^{-3} (provided by the manufacturer) and an equilibrium contact angle (air–water–lawn of colloids) of 115.2° (measured with a Tantec Contact Angle Meter, Tantec Inc., Schaumburg, IL). Specific physical and chemical characteristics for the 1.0-μm particles include: surface charge density of 27 μC cm^{-2} (provided by manufacturer) and zeta potential of −83.5 mV (measured with a Zetasizer 3000, Malvern Instruments, Inc., Southborough, MA). In contrast, the 3.2-μm particles had a surface charge density of 11.9 μC cm^{-2} and a zeta potential of −85.5 mV. The initial influent concentration (C_i) for the 1.0- and 3.2-μm colloids was equal to 3.86×10^{10} N$_c$ L^{-1} (where N$_c$ denotes number of colloids) and 1.18×10^9 N$_c$ L^{-1}, respectively.

The aqueous phase chemistry (pH, ionic strength, and composition) of the tracer, resident, and eluant solutions utilized in the soil column experiments was chosen to create a stabilized monodispersed suspension with the selected colloids. The initial resident and eluant solutions consisted of 0.001 M NaCl with its pH buffered to 6.98 using NaHCO$_3$ (5×10^{-5} M). The colloid-conservative tracer solution consisted of 0.001 M NaBr with its pH buffered to 6.73 using NaHCO$_3$ (5×10^{-5} M) and the previously indicated initial colloid concentration. The aqueous solvent for all experimental solutions consisted of deionized water.

Aquifer material used for the soil column experiments consisted of various sieve sizes of Ottawa (quartz) sand (U.S. Silica, Ottawa, IL). The porous media were selected to encompass a range in grain sizes and were designated by their median grain size (d_{50}) as 710, 360, 240, and 150 μm. Specific properties of the 710-, 360-, 240-, and 150-μm sands, include: uniformity index (d_{60}/d_{10}; here x% of the mass is finer than d_x) of 1.21, 1.88, 3.06, and 2.25; and intrinsic permeability of 4.08×10^{-10}, 6.37×10^{-11}, 1.12×10^{-11}, and 4.68×10^{-12} m^2, respectively. The pore size distribution for these Ottawa sands can be estimated from capillary pressure–saturation curves presented by Bradford and Abriola (2001). Ottawa sands typically consisted of 99.8% SiO$_2$ (quartz) and trace amounts of metal oxides,

were spheroidal in shape, and had rough surfaces. The vast majority of the sands possessed a net negative charge at a neutral pH.

Aluminum soil columns, 10 cm long and with a 5-cm inside diameter, were used in the transport studies. The columns were equipped with standard fittings at both of their ends. A stainless-steel wire screen (105-μm mesh spacing) was placed at the soil surfaces to avoid sand displacement. Tubing to and from the columns, fittings, and column o-rings were composed of chemically resistant materials such as teflon, viton, and stainless steel.

The heterogeneous systems consisted of two soil types, a soil cylinder (2.3-cm diameter, 6 cm long) lens embedded in the center of a second soil referred to as the matrix. The soil columns were wet packed with the various porous media, with the water level kept above the soil surface. Care was taken to ensure uniform packing by thoroughly mixing small quantities of the appropriate sieve size before addition to the columns. After each incremental addition of soil, the added soil was gently mixed with the lower surface layer of soil and then vibrated to minimize settling and layering, and to liberate any entrapped air. After filling the soil column to a height of 2 cm with the matrix soil, a stainless-steel cylinder of 2.3-cm internal diameter was gently placed in the middle of the soil column. The sand forming the heterogeneity (lens) was filled inside the cylinder while matrix soil was added to the space separating the outer column and interior cylinder to the same height as the soil lens. When the interior cylinder was filled to a height of 6 cm (8 cm above the base of the column), the interior cylinder was gently removed from the column and the remaining column space was filled with matrix soil. Table 1 provides porosity (ε) values for each experimental soil column. The porosity was determined according to the method of Danielson and Sutherland (1986) using the measured soil bulk density and assuming a specific solid density of 2.65 g cm^{-3}.

Before initiating a carboxyl colloid tracer experiment the soil columns containing Ottawa sand were flushed with several cycles of deionized water and 0.026 M NaCl to remove most of the natural colloids particles from the porous media. The soil columns were flushed as follows: initial resident solution was 0.026 M NaCl, 2 pore volume (PV) flush with deionized water, 2 PV flush with 0.026 M NaCl solution, 2 PV flush with deionized water, and finally a 4 PV flush with eluant solution. Here the 0.026 M NaCl solution promotes clay aggregation and the deionized water promotes clay mobilization (Bettahar et al., 1998). This treatment produced persistently low effluent concentrations of natural colloids in the column effluent.

A Masterflex L/S multihead drive pump (Barnant Company, Barrington, IL) was used to pump colloid and bromide

tracer or eluant solution upward through the vertically oriented columns at a steady rate. The average Darcy velocity (q) for the various soil column experiments is given in Table 1. The colloid and bromide tracer solutions were pumped through the columns for about 81 min, after which a three-way valve was used to switch the pumped solution to the eluant for a total experimental time of 250 min. A total of 50 effluent samples were collected and analyzed for colloid and bromide concentration using a Turner Quantech Fluorometer (Barnstead/Thermolyne, Dubuque, IA) and an Orion 720a pH/ISE meter (Orion Research Inc., Beverly, MA), respectively. The analytic protocol was sensitive to concentrations over approximately two orders of magnitude below the initial colloid and bromide concentrations. Concentrations of the 3.2-μm colloids were slightly influenced by background interference from natural colloids (<3% of C/C_i).

Following completion of the colloid transport experiments, the spatial distribution of colloids in a soil column was determined. The end fitting was removed and the saturated sand was carefully excavated into 20-mL scintillation vials from the column outlet to inlet. Excess eluant solution was added to the vials. The vials were slowly shaken for 4 h using a Eberbach shaker (Eberbach Corporation, Ann Arbor, MI) to liberate retained colloids. The concentration of the colloids in the excess aqueous solution was measured with a Turner Quantech Fluorometer using the same experimental protocol as followed for the effluent samples. These concentrations were corrected for colloid release efficiency (determined from batch experiments) and natural background colloids (determined from replicate "blank" soil columns). Additional details on the experimental protocols and procedures that were used to determine the spatial distribution of retained colloids are given by Bradford et al. (2002).

A colloid mass balance was conducted at the end of each soil column experiment using effluent concentration data and the final spatial distribution of retained colloids in the sands. The calculated number of effluent and soil colloids was normalized by the total number of injected particles into a column. Table 1 presents the calculated effluent (M_e), soil (M_s), and the total ($M_t = M_e + M_s$) colloid mass fractions recovered for the experimental systems. To account for mass balance errors in the experimental data, the concentration of colloids retained in the sand was multiplied by $(1 - M_e)/M_s$. This approach assumes that the colloid mass balance error occurs primarily on the solid phase.

THEORY AND MODEL

Clean-bed colloid attachment–detachment theory has frequently been used to describe colloid interactions with porous media as (e.g., Bolster et al., 1999; Tufenkji et al., 2003):

$$\frac{\partial(\rho_b S_{att})}{\partial t} = \theta_w k_{att} C - \rho_b k_{det} S_{att} \qquad [1]$$

Here t is time (T), ρ_b (M L^{-3}) is the soil bulk density, S_{att} (N$_c$ M^{-1}—N$_c$ denotes number of colloids) is the solid phase concentration of attached colloids, θ_w is the volumetric water content, k_{att} (T^{-1}) is the first-order colloid attachment coefficient, k_{det} (T^{-1}) is the first-order colloid detachment coefficient, and C (N$_c$ L^{-3}) is the liquid phase colloid concentration. Colloid filtration theory is incorporated into the k_{att} term as (e.g., Logan et al., 1995):

$$k_{att} = \frac{3(1 - \theta_w)}{2 d_{50}} \eta \alpha v \qquad [2]$$

where η is the collector (porous medium) efficiency, α is the

Table 1. Soil column properties (porosity, ε; and Darcy water velocity, q_w) and the recovered effluent (M_e), soil (M_s), and total colloid mass fraction (M_t).

Soil matrix	Soil lens	d_p	ε	q_w	M_e	M_s	M_t
		μm		cm min^{-1}			
710	360	1.0	0.323	0.121	0.613	0.218	0.831
710	240	1.0	0.328	0.109	0.614	0.198	0.812
710	150	1.0	0.329	0.127	0.636	0.198	0.834
710	360	3.2	0.320	0.126	0.607	0.491	1.098
710	240	3.2	0.320	0.102	0.505	0.583	1.088
710	150	3.2	0.339	0.129	0.536	0.499	1.035
360	710	1.0	0.309	0.095	0.585	0.242	0.827
240	710	1.0	0.307	0.117	0.532	0.315	0.847
150	710	1.0	0.329	0.106	0.435	0.431	0.866
360	710	3.2	0.318	0.120	0.297	0.594	0.891
240	710	3.2	0.321	0.108	0.221	0.831	1.052
150	710	3.2	0.328	0.115	0.148	1.109	1.257

colloid sticking efficiency, d_{50} (L) is the median porous medium grain diameter, and v (L T^{-1}) is the pore water velocity. In this work the value of η is calculated using the following correlation written in terms of dimensionless variables (Logan et al., 1995; Rajagopalan and Tien, 1976):

$$\eta = 4 A_s^{1/3} N_{Pe}^{-2/3} + A_s N_{Lo}^{1/8} N_R^{15/8} +$$
$$0.00338 A_s N_G^{1.2} N_R^{-0.4} \quad [3]$$

Here A_s is the Happel correction factor, N_{Pe} is the Peclet number, N_{Lo} is London-van der Waals attractive forces number, N_R is the interception number, and N_G is the gravitional number. The first, second, and third terms on the right-hand side of Eq. [3] denote contributions due to diffusion, interception, and sedimentation, respectively (Logan et al., 1995). The value of α in Eq. [2] represents the fraction of particles colliding with the porous medium that remains attached and therefore reflects the net effect of repulsive and attractive forces between colloids and solid surfaces. The value of α is usually derived from experimental breakthrough curves (Pieper et al., 1997; Ryan et al., 1999) or from fitted values of k_{att} and calculated values of η (Bales et al., 1991; Redman et al., 1997).

Straining is modeled according to a slightly modified form of the approach described in Bradford et al. (2003). The mass balance equation for strained colloids is given as:

$$\frac{\partial(\rho_b S_{str})}{\partial t} = \theta_w k_{str} \psi_{str} C \quad [4]$$

where k_{str} (T^{-1}) is the straining coefficient, ψ_{str} is a dimensionless colloid straining function, and S_{str} (N$_c$ m^{-1}) is the solid phase concentration of strained colloids. The value of ψ_{str} is a function of distance and is described as

$$\psi_{str} = H(z - z_o)\left(\frac{d_{50} + z - z_0}{d_{50}}\right)^{-\beta} \quad [5]$$

where β is a parameter that controls the shape of the colloid spatial distribution, $H(z - z_o)$ is the Heaviside function, z (L) is depth, and z_o (L) is the depth for the column inlet (matrix sand) or textural interface (lens sand). Equation [5] assumes that colloid mass retention by straining occurs primarily at the column inlet or textural interface because colloids are retained in dead-end pores that are smaller than some critical size. The number of dead-end pores is hypothesized to decrease with increasing distance because size exclusion and/or limited transverse dispersivity tend to keep mobile colloids within the larger networks, thus bypassing smaller pores. Bradford et al. (2003) found that the value of $\beta = 0.432$ gave a good description of the spatial distribution of retained colloids when significant straining occurred. For the remainder of this manuscript β will be fixed to this value. In contrast to the attachment–detachment model given by Eq. [1] through [3], the straining model does not include a dependence on velocity. Additional studies are warranted to quantify the velocity dependence of the straining coefficient.

Mathematical modeling of water flow and bromide and colloid transport in the experimental systems was conducted using a modified version of the HYDRUS-2D computer code (Simunek et al., 1999). To simulate the three-dimensional flow and transport process that occurred in the heterogeneous systems considered in this work, the code was run in axisymmetric (r-z) mode. This code was modified to account for colloid attachment and detachment (Eq. [1]–[3]), and straining (Eq. [4] and [5]). Although attachment and straining are likely to occur simultaneously in natural systems, these processes were considered separately in this work to facilitate the determination of unique parameter estimates in the heterogeneous sys-

tems. The incomplete characterization of the velocity dependence of colloid retention parameters (especially straining parameters) also hindered the simultaneous description of attachment and straining.

Bradford et al. (2003) presented a method to predict the influence of size and anion exclusion on colloid transport. The influence of exclusion becomes more apparent with increasing transport distances. Because of the relatively small transport distances considered in this work (10 cm), exclusion was not simulated. Bromide and colloids are therefore both assumed to be transported at the same pore water velocity.

To minimize the number of parameters that were fitted to the heterogeneous systems, the detachment coefficient and the bromide and colloids hydrodynamic longitudinal dispersivities (λ_H^{BR} and λ_H) that were used in the simulations were taken from homogeneous soil column studies that employed the same sands and colloids (Bradford et al., 2002). Table 2 summarizes these parameter values. The transverse dispersivity was set equal to one-tenth of the longitudinal dispersivity. Bradford et al. (2002) discussed differences in the bromide and colloid dispersivity for a particular sand. The detachment coefficients (Table 2) were quite low and had only a minor influence on the homogeneous colloid transport experiments.

HYDRUS-2D is coupled to a nonlinear least squares optimization routine based upon the Marquardt–Levenberg algorithm (Marquardt, 1963) to facilitate the estimation of colloid transport parameters from experimental data. Each model simulation was obtained by simultaneously fitting two parameters to effluent and retention data collected from a heterogeneous colloid transport experiment. Sticking efficiencies (independent of velocity) for the matrix and lens sands were fitted for the attachment model (Eq. [1]–[3]). Attachment coefficients were not directly fitted, so that the velocity dependence of k_{att} could be characterized (Eq. [2] and [3]). Straining coefficients for the matrix and lens sands were fitted for the straining model (Eq. [4] and [5]).

RESULTS AND DISCUSSION
Transport in Heterogeneous Systems: 710-μm Matrix

We first discuss the water flow and transport of bromide and colloids through the physically heterogeneous systems consisting of a finer-textured sand (360, 240, and 150 μm) lens embedded in the center of 710-μm matrix sand. In these systems the finer-textured lens has a lower intrinsic permeability than the coarser-textured 710-μm matrix. Figure 1 presents the simulated aqueous phase velocity distribution in the 710-μm matrix–360-μm lens system. The higher permeability of the matrix

Table 2. Transport parameters (bromide dispersivity, λ_H^{BR}; colloid dispersivity, λ_H; and detachment coefficient, k_{det}) that were obtained from homogeneous soil column data (Bradford et al., 2002).
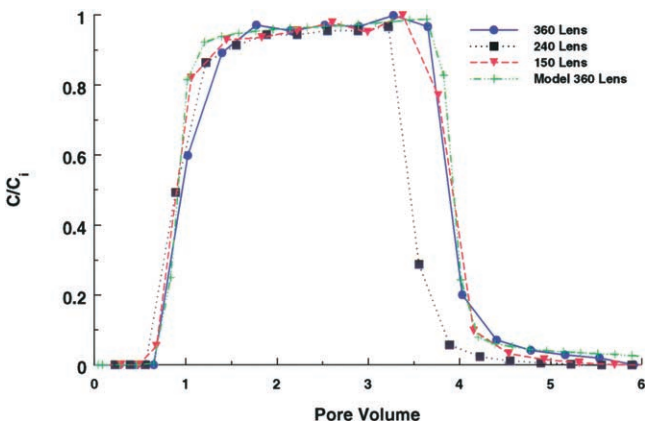
Soil type	d_p	λ_H^{BR}	λ_H	$k_{det} \times 10^4$
	μm	cm		min^{-1}
710	1.00	0.061	0.237	0.75
710	3.20	0.076	0.239	4.10
360	1.00	0.070	0.158	6.65
360	3.20	0.103	0.288	2.87
240	1.00	0.074	0.179	10.0
240	3.20	0.053	0.361	3.75
150	1.00	0.080	0.071	12.4
150	3.20	0.179	0.299	12.0
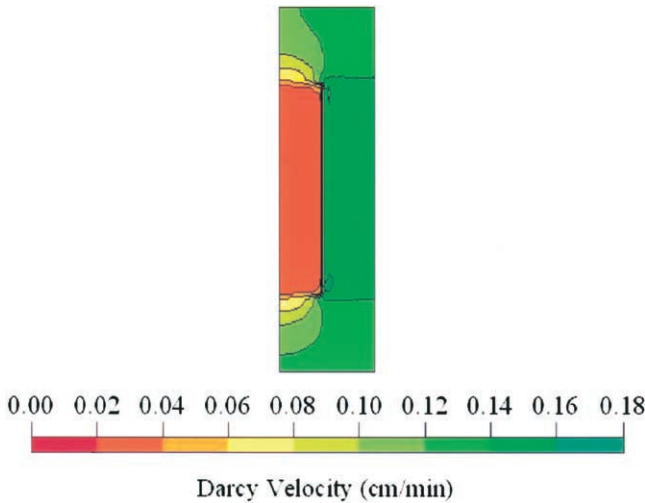
Fig. 1. **Simulated aqueous phase velocity distribution in the 710-μm matrix–360-μm lens system. A cross-section view from the column center (left) to the column boundary (right) is shown.**

leads to significant flow bypassing of the finer-textured lens material. An estimate of the volume fraction of water that passes through the lens was calculated from the ratio of the transmissivity (product of the cross-sectional area and hydraulic conductivity) for the lens material and the total column to be 4.0, 0.7, and 0.3% for the 360-, 240-, and 150-μm lens systems, respectively. Hence, more than 96% of the water flows through the 710-μm matrix sand in these systems.

Figure 2 shows a plot of the effluent concentration curves (relative concentration, C/C_i, as a function of pore volume) for bromide in the indicated 710-μm matrix systems. Observe that the initial breakthrough of bromide occurs slightly before one pore volume (about 0.85–0.9 PV), due to flow bypassing of the lens. The somewhat asymmetric shape (approach to peak effluent concentration, and tailing) of the bromide breakthrough curve is also controlled by the degree of water bypassing (Fig. 1). In general, the transport behavior of bromide in the various 710-μm matrix systems is quite similar because comparable amounts of water bypass the various soil lenses. Variations in the bromide (and colloid) pulse volume occurred as a result of differences in the

Darcy velocity for the columns (Table 1). Figure 2 also presents the simulated effluent concentration curve for bromide in the 710-μm matrix–360-μm lens system. The predicted bromide effluent concentration curve is very similar to the observed data. This suggests that the bromide transport parameters and the simulated aqueous phase flow field (Fig. 1) accurately characterize the experimental conditions.

Figures 3a and 3b present plots of the 1.0-μm colloid effluent concentration curves and the spatial distributions of retained colloids in the indicated 710-μm matrix systems. The relative effluent concentrations are plotted as a function of pore volumes in Fig. 3a. In Fig. 3b the normalized concentration (number, N_c, divided by the total number added to the column, N_{tc}) per gram of dry sand is plotted as a function of dimensionless depth from the column inlet. The beginning and ending locations for the lens sand are denoted with solid horizontal lines in figures of the colloid spatial distributions. The 1.0-μm colloid transport behavior is very similar for the different heterogeneous systems. This observation is consistent with the similar water flow and bromide transport shown in Fig. 1 and 2, respectively. Similar to bromide (Fig. 2), the earlier colloid breakthrough occurs as a result of flow bypassing of the finer-textured lenses (Fig. 1). Figure 3b indicates that the majority of the colloid mass removal occurs near the inlet interface of the matrix and the fine-textured lens. This likely occurs as a

Fig. 2. **Observed and simulated (710-μm matrix–360-μm lens) effluent concentration curves of bromide in the indicated 710-μm matrix systems.**
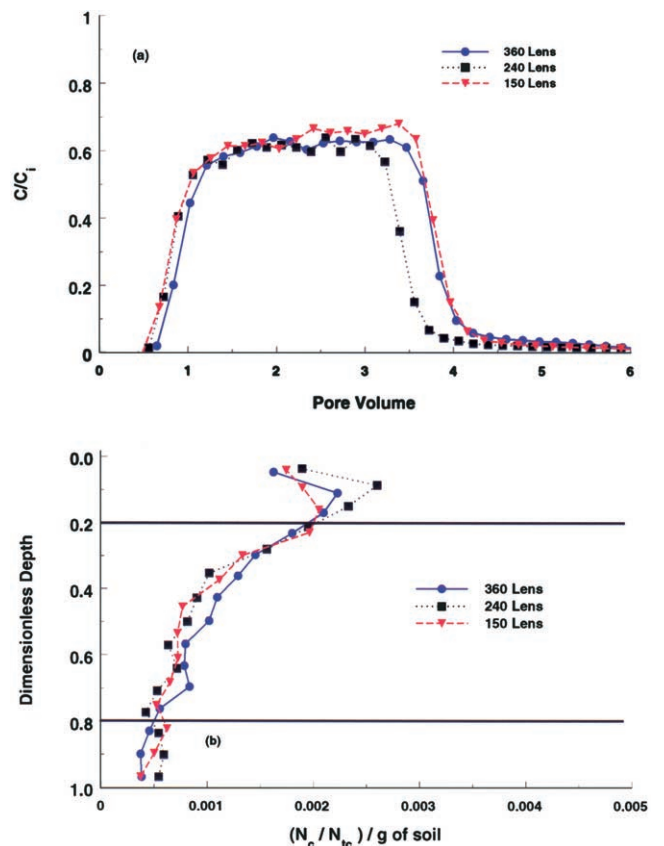
Fig. 3. **(a) The effluent concentration curves and (b) the final spatial distributions of 1.0-μm colloids in the indicated 710-μm matrix systems.**
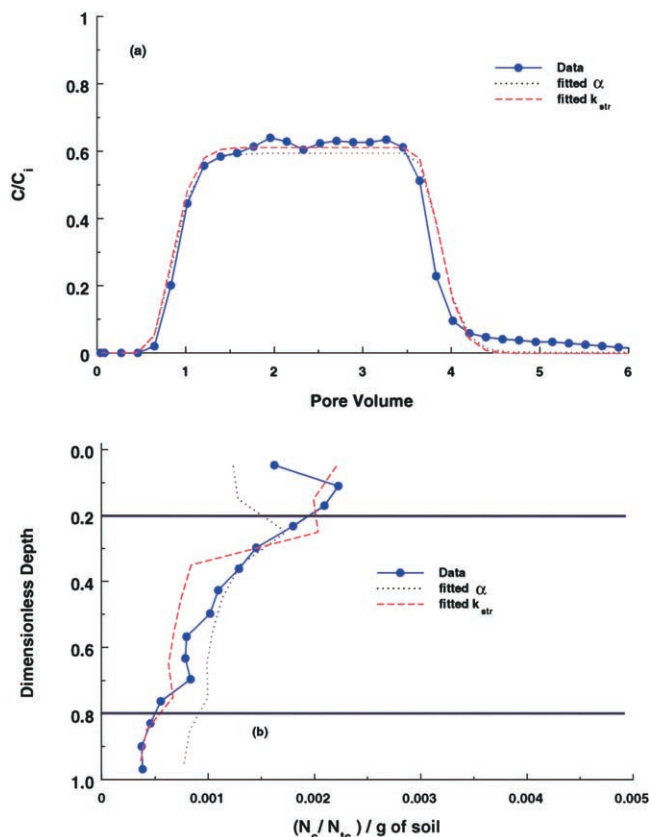
Fig. 4. Observed and simulated (parameters for the attachment and straining models are given in Table 3) (a) effluent concentration curves and (b) the final spatial distributions of 1.0-μm colloids in the 710-μm matrix–360-μm lens system.

result of variations in colloid retention with changes in the aqueous flow field in this region (Fig. 1) or due to enhanced retention in the finer-textured sand lens.

Figures 4a and 4b present plots of the observed and simulated (attachment and straining models) 1.0-μm colloid effluent concentration curves and the spatial distributions of retained colloids in the 710-μm matrix–360-μm lens system. Table 3 shows fitted parameter values for the attachment (Eq. [1]–[3]) and straining

(Eq. [4] and [5]) models, and statistical parameters (coefficient of linear regression, and standard error) for the goodness of parameter fit. Uncertainty in the estimated colloid transport parameters in the finer-textured lens sand is quite large due to flow bypassing of this material. Both the attachment and straining models provide a reasonable description of the effluent concentration curve and the spatial distribution of retained colloids. Analysis of homogeneous transport data for 1.0-μm colloids in the 710-μm sand by Bradford et al. (2003), however, indicates that attachment is likely the dominant retention process.

Figures 5a and 5b present plots of the 3.2-μm colloid effluent concentration curves and the spatial distributions of retained colloids in the indicated 710-μm matrix systems. As for the 1.0-μm colloids (Fig. 3a) and bromide (Fig. 2), the transport and retention behavior for the 3.2-μm colloids is similar for the different soil heterogeneities. We again attribute this to the fact that most of the water flows through the 710-μm matrix material (>96%) and bypasses much of the finer-textured lens (Fig. 1). Comparison of Fig. 3 and 5 reveals lower effluent concentrations and greater mass retention near the column inlet for the 3.2-μm colloids than for the 1.0-μm colloids. Figures 6a and 6b present plots of the observed and simulated 3.2-μm colloid effluent concentration curves and the spatial distributions of retained colloids in the 710-μm matrix–360-μm lens system. Fitted parameters from the attachment and straining models are summarized in Table 3. Considerable uncertainty in the estimated transport parameters for the finer-textured lens sand occurred as a result of flow bypassing. The attachment model provides an adequate description of the effluent concentration curve, but does not satisfactorily describe the spatial distribution of retained colloids. The straining model provides a slightly improved characterization of the spatial distribution. Data analysis by Bradford et al. (2003) indicates that transport of 3.2-μm colloids in homogeneous 710-μm sand was controlled by straining. This hypothesis was supported by the systematic trends of increasing colloid retention with increasing colloid size or decreasing median sand grain size, the

Table 3. Fitted parameters (sticking efficiency, α; and straining coefficient, k_{str}) from the attachment (Eq. [1]–[3]) and straining (Eq. [4] and [5]) models.

| Figure	Model	d_p	Sand	Symbol	Units	Fit	SE	r^2
		μm						
4	Attach	1.0	710†	α	–	0.173	0.012	0.969
			360‡	α	–	0.491	0.218	
4	Strain	1.0	710†	k_{str}	min^{-1}	0.065	0.005	0.978
			360‡	k_{str}	min^{-1}	2.000	1.053	
6	Attach	3.2	710†	α	–	0.160	0.010	0.924
			360‡	α	–	0.043	0.052	
6	Strain	3.2	710†	k_{str}	min^{-1}	0.108	0.007	0.932
			360‡	k_{str}	min^{-1}	0.441	0.244	
10	Attach	1.0	710‡	α	–	0.001	0.241	0.743
			150†	α	–	0.266	0.041	
10	Strain	1.0	710‡	k_{str}	min^{-1}	0.000	0.073	0.938
			150†	k_{str}	min^{-1}	0.323	0.023	
12	Attach	3.2	710‡	α	–	0.031	0.624	0.855
			150†	α	–	0.867	0.123	
12	Strain	3.2	710‡	k_{str}	min^{-1}	0.021	0.179	0.988
			150†	k_{str}	min^{-1}	1.160	0.054	

† Denotes matrix sand.
‡ Denotes lens sand.
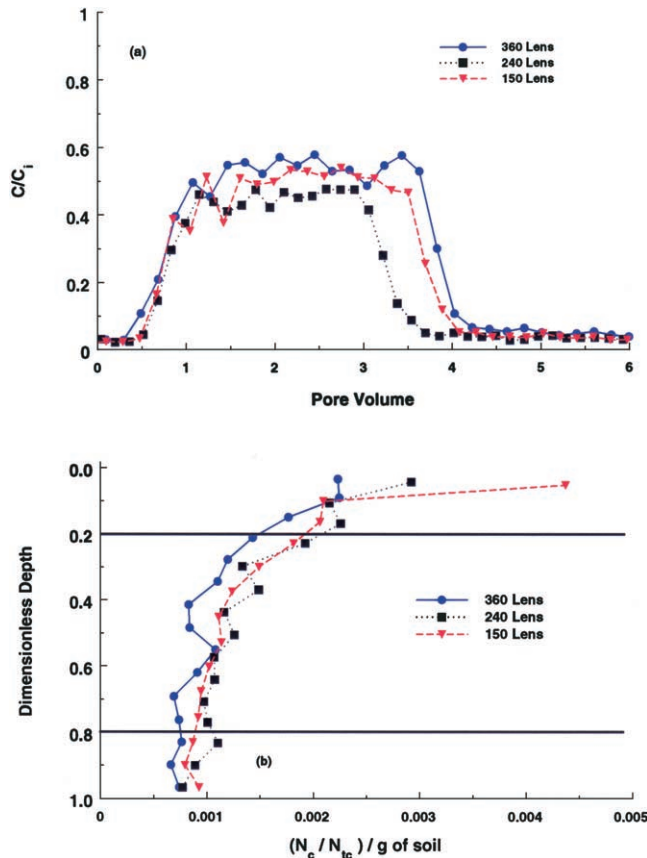
Fig. 5. (a) The effluent concentration curves and (b) the final spatial distributions of 3.2-μm colloids in the indicated 710-μm matrix systems.
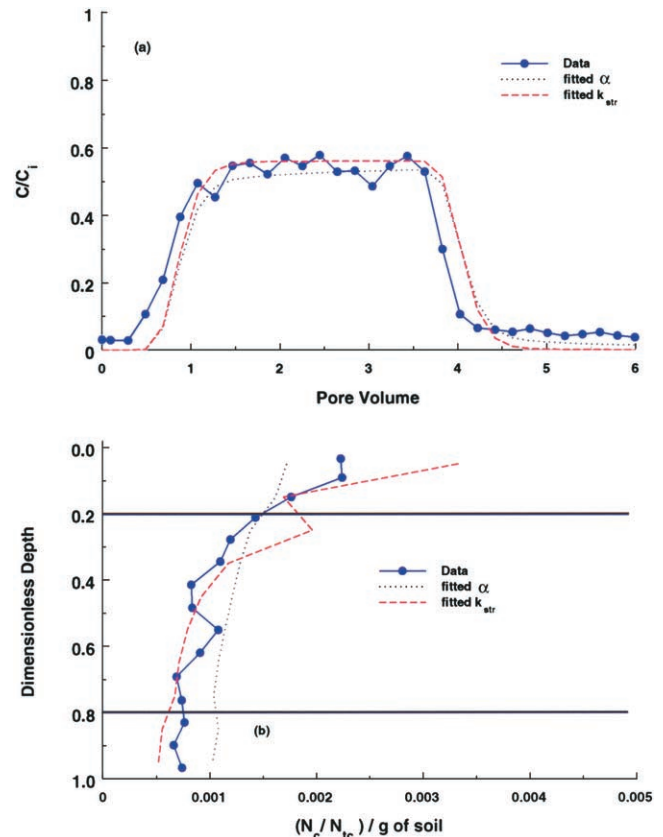

Fig. 6. Observed and simulated (parameters for the attachment and straining models are given in Table 3) (a) effluent concentration curves and (b) the final spatial distributions of 3.2-μm colloids in the 710-μm matrix–360-μm lens system.

inability of conventional attachment or blocking theory to accurately characterize the colloid spatial distribution, and the wide variability (a factor of 24) in fitted sticking efficiencies for a given porous medium and for colloids that had similar surface charges but different sizes.

It should also be mentioned that the 3.2-μm colloids in the 710-μm matrix–360-μm lens system exhibited slightly earlier colloid breakthrough (Fig. 5) compared with bromide (Fig. 2). This observation is attributed to size exclusion and/or the greater dispersivity of colloid particles compared with bromide (Table 2). This behavior, however, was not observed for the 710-μm matrix systems containing 240- or 150-μm lens, presumably due to greater flow bypassing of the finer-textured lens sands.

Transport in Heterogeneous Systems—710-μm Lens

This section discusses water flow, and the transport of bromide and colloids, through the physical heterogeneous systems consisting of a 710-μm sand lens embedded in the center of the finer-textured (360, 240, and 150-μm) matrix sand. In these systems the finer-textured matrix sand has a lower water permeability than the coarser-textured 710-μm lens. Figure 7 presents the simulated aqueous phase velocity distribution in the 710-μm lens–360-μm matrix system. Notice that water flows

preferentially through the lens and tends to bypass a large volume of finer-textured matrix material adjacent to the lens in the middle region of the column. An estimate of the volume fraction of water that passes through the lens was calculated from the ratio of the transmissivity for the lens material and the total column to be 63.0, 90.7, and 95.7% for the 360-, 240-, and 150-μm
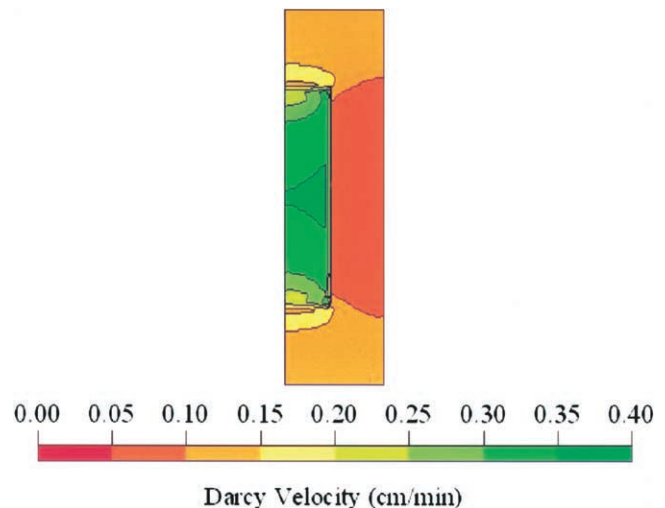

Fig. 7. Simulated aqueous phase velocity distribution in the 710-μm lens–360-μm matrix system. A cross-section view from the column center (left) to the column boundary (right) is shown.

matrix systems, respectively. Hence, the trend of decreasing water permeability with decreasing median grain size of the matrix material promotes increased bypassing of the matrix material near the lens in these physically heterogeneous systems.

Figure 8 presents plots of the effluent concentration curves for bromide in the indicated 710-μm lens systems. Due to pronounced flow bypassing in these systems (Fig. 7), the bromide breakthrough occurs considerably earlier than one pore volume (between 0.6 and 0.85), and the effluent curves are asymmetrically shaped (slow approach to peak effluent concentration and tailing). Differences in the bromide effluent curves occur primarily as a result of the variations in the volume of water that is transported in the 710-μm lens material. A simulated effluent concentration curve for bromide in the 360-μm matrix–710-μm lens system is also presented in Fig. 8. The observed and predicted bromide effluent concentration curves exhibit reasonable agreement, indicating that the bromide transport parameters and simulated aqueous phase flow field (Fig. 7) are accurately characterized.

Figure 9a presents the effluent concentration curves for 1.0-μm colloids in the indicated heterogeneous 710-μm lens systems. The peak effluent concentration decreases with decreasing matrix grain size (360 > 240 > 150 μm). The spatial distributions of retained 1.0-μm colloids in the various 710-μm lens systems are shown in Fig. 9b. The 150-μm matrix system has the highest colloid concentrations at the column inlet and then decreases rapidly to a low constant concentration with increasing dimensionless depth. The spatial distribution of colloids in the 360-μm matrix system has a much more gradual shape and higher colloid concentrations directly below the inlet lens–matrix interface (at a dimensionless depth of 0.3) compared with the 150-μm matrix system. The 240-μm matrix systems exhibit intermediate behavior to the 360- and 150-μm matrix systems. Both effluent and spatial distribution data are consistent with straining, which increases in magnitude and frequency with decreasing grain size of the sand.
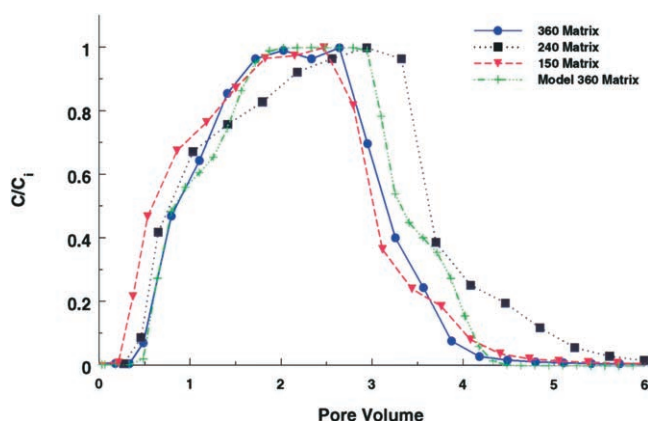

Fig. 8. Observed and simulated (710-μm lens–360-μm matrix) effluent concentration curves of bromide in the indicated 710-μm lens systems.

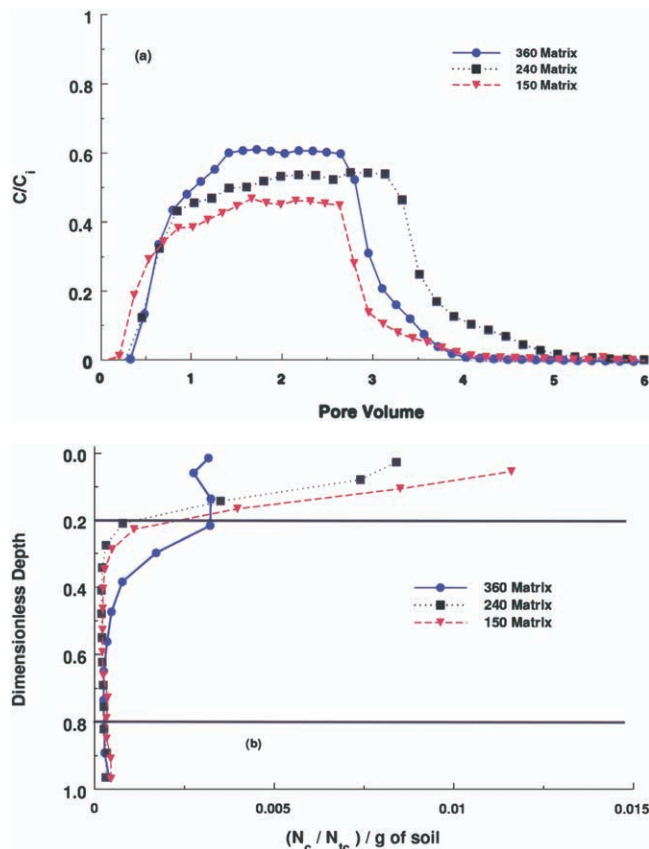**Fig. 9. (a) The effluent concentration curves and (b) the final spatial distributions of 1.0-μm colloids in the indicated 710-μm lens systems.**

Figures 10a and 10b present plots of the observed and simulated 1.0-μm colloid effluent concentration curves and the spatial distributions of retained colloids in the 150-μm matrix–710-μm lens system. Table 3 summarizes the fitted parameters from the attachment and straining models. The sticking efficiency for the 150-μm matrix sand was 266 times greater than that for the 710-μm lens sand. This difference is physically unrealistic because α is theoretically the same for similar Ottawa sands and colloids. In comparison with the attachment model, the straining model provides an improved characterization of the effluent concentration curve and the spatial distribution. This observation suggests that straining is an important mechanism of colloid retention for the 1.0-μm colloids in this system. Straining also likely influences the retention of 1.0-μm colloids in the other 710-μm lens systems (360- and 240-μm matrix sands), but to a lesser extent due to the larger median grain size of the matrix sand in these systems. Attachment is anticipated to have a greater role in colloid retention for coarser-textured sands and/or smaller colloids.

Figure 11a presents the effluent concentration curves for the 3.2-μm colloids in the heterogeneous 710-μm lens systems. As for the 1-μm colloids (Fig. 9a), the 3.2-μm colloids follow a trend of decreasing peak effluent concentration with decreasing matrix grain size (360 > 240 > 150 μm). The corresponding 3.2-μm col-
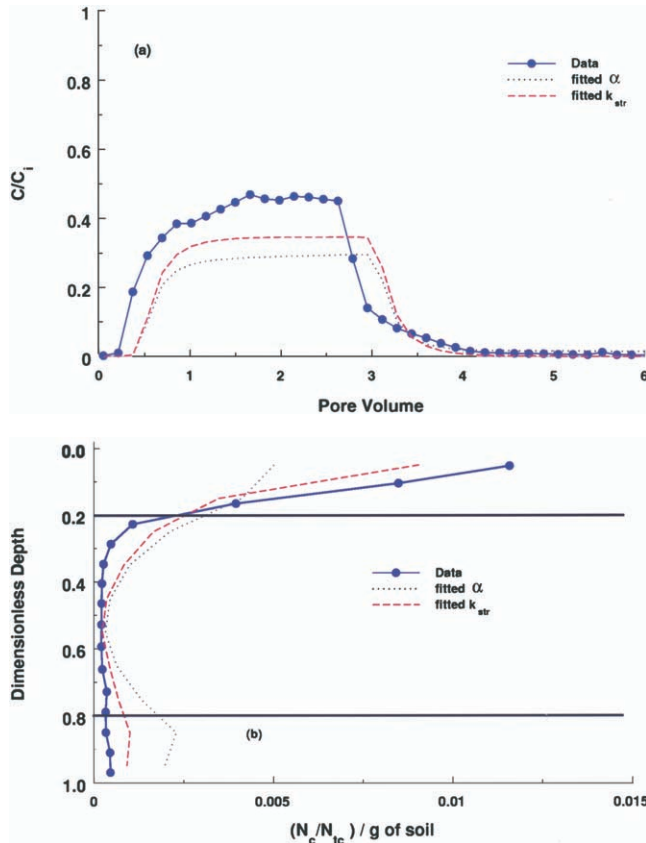
Fig. 10. Observed and simulated (parameters for the attachment and straining models are given in Table 3) (a) effluent concentration curves and (b) the final spatial distributions of 1.0-μm colloids in the 710-μm lens–150-μm matrix system.

Fig. 11. (a) The effluent concentration curves and (b) the final spatial distributions of 3.2-μm colloids in the indicated 710-μm lens systems.

loid spatial distribution plots are shown in Fig. 11b. The heterogeneous 710-μm lens systems exhibits high concentrations in the sand near the inlet and then rapidly decreases to a constant low value with increasing distance until a dimensionless depth of around 0.6. A second minor increase in colloid retention occurs near the interface of the lens and matrix sands in the 240- and 150-μm matrix systems (dimensionless depth of around 0.6). For a particular matrix sand and 710-μm lens system, comparison of Fig. 9 and 11 reveals lower effluent concentrations and greater mass retention near the column inlet for the 3.2-μm colloids than for the 1.0-μm colloids. This observation is consistent with straining behavior, which is more pronounced for larger colloids (Bradford et al., 2002).

Figures 12a and 12b present plots of the observed and simulated 3.2-μm colloid effluent concentration curves and the spatial distributions of retained colloids in the 150-μm matrix–710-μm lens system. Table 3 summarizes the fitted parameters from the attachment and straining models. The difference in the fitted sticking efficiencies for the 150-μm matrix (28 times greater) and 710-μm lens sands was physically unrealistic since α is theoretically the same for similar Ottawa sands and colloids. Similar to Fig. 10b, the straining model provided an improved description of both the effluent
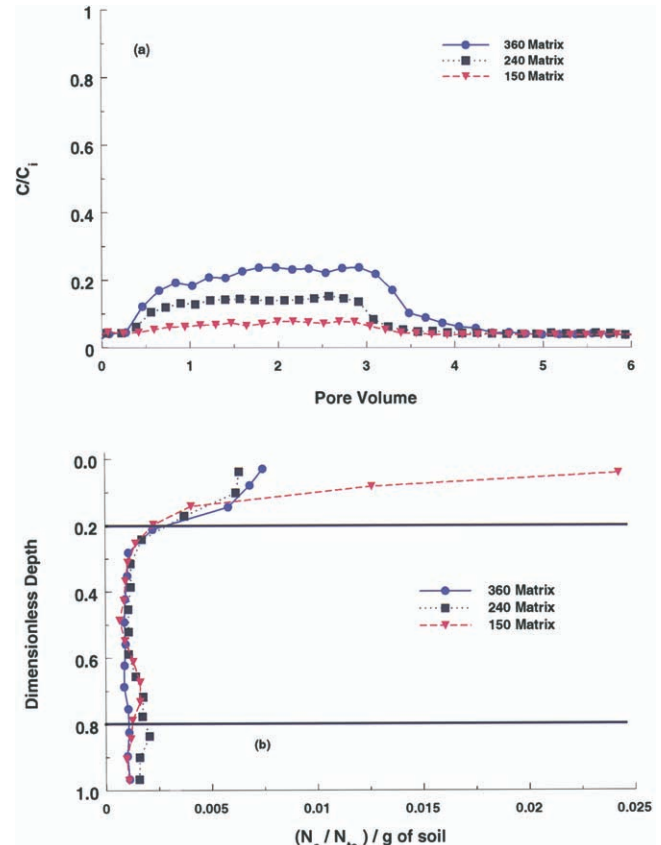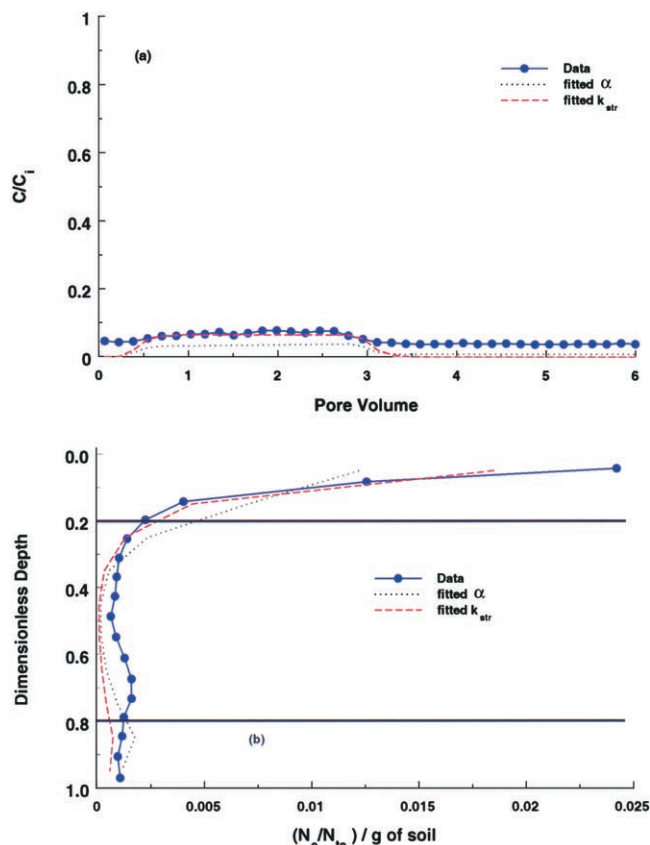
concentration curve and the spatial distribution compared with the attachment model. This observation suggests that straining is an important mechanism of colloid retention for the 3.2-μm colloids in this system, as well as the other 710-μm lens systems (360- and 240-μm matrix sands).

SUMMARY

Colloid transport studies were conducted in water-saturated physically heterogeneous systems to gain insight into the processes controlling transport in natural aquifer and vadose zone (variably saturated) systems. Attachment is typically assumed to be the dominant mechanism of colloid retention in porous media. The experimental results and analysis in this manuscript indicate that straining is also sometimes an important mechanism of colloid retention, especially for decreasing median grain size and increasing colloid size. Straining was found to be greatest in sand adjacent to the column inlet, whereas attachment likely occurred throughout the system at a lower rate. Results from this study were consistent with the finding reported in Bradford et al. (2003) that straining was a significant mechanism of colloid retention for values of $(d_p/d_{50}) > 0.005$. This work also underlines the importance of aqueous phase velocity distribution, retention at interfaces of textural contrast, and exclusion in heterogeneous systems. Additional research is warranted to better characterize the

Fig. 12. Observed and simulated (parameters for the attachment and straining models are given in Table 3) (a) effluent concentration curves and (b) the final spatial distributions of 3.2-μm colloids in the 710-μm lens–150-μm matrix system.

dependence of attachment and, especially, straining on these factors. The potential role of attachment as a means to initiate straining also needs to be examined.

REFERENCES

Abu-Sharar, T.M., F.T. Bingham, and J.D. Rhoades. 1987. Stability of soil aggregates as affected by electrolyte concentration and composition. Soil Sci. Soc. Am. J. 51:309–314.

Bales, R.C., S.R. Hinkle, T.W. Kroeger, and K. Stocking. 1991. Bacteriophage adsorption during transport through porous media: Chemical perturbations and reversibility. Environ. Sci. Technol. 25:2088–2095.

Bales, R.C., S. Li, K.M. Maguire, M.T. Yahya, and C.P. Gerba. 1993. MS-2 and poliovirus transport in porous media: Hydrophobic effects and chemical perturbations. Water Resour. Res. 29:957–963.

Bettahar, M., O. Razakarisoa, F. van Dorpe, and M. Baviere. 1998. Influence of a surfactant contamination technique on the hydraulic conductivity of a controlled aquifer polluted by diesel. Rev. Sci. L'Eau 11:85–100.

Bitton, G., and R.W. Harvey. 1992. Transport of pathogens through soil. p. 103–124. In R. Mitchell (ed.) New concepts in environmental microbiology. Wiley-Liss, New York.

Bolster, C.H., A.L. Mills, G.M. Hornberger, and J.S. Herman. 1999. Spatial distribution of bacteria experiments in intact cores. Water Resour. Res. 35:1797–1807.

Bradford, S.A., and L.M. Abriola. 2001. Dissolution of residual tetrachloroethylene in fractional wettability porous media: Incorporation of interfacial area estimates. Water Resour. Res. 37:1183–1195.

Bradford, S.A., S.R. Yates, M. Bettahar, and J. Simunek. 2002. Physical factors affecting the transport and fate of colloids in saturated porous media. Water Resour. Res. 38(12):1327 DOI: 10.1029/2002WR001340.

Bradford, S.A., J. Simunek, M. Bettahar, M.Th. van Genuchten, and S.R. Yates. 2003. Modeling colloid attachment, straining, and exclusion in saturated porous media. Environ. Sci. Technol. 37:2242–2250.

Camesano, T.A., and B.E. Logan. 1998. Influence of fluid velocity and cell concentration on the transport of motile and nonmotile bacteria in porous media. Environ. Sci. Technol. 32:1699–1709.

Cumbie, D.H., and L.D. McKay. 1999. Influence of diameter on particle transport in a fractured shale saprolite. J. Contam. Hydrol. 37:139–157.

Danielson, R.E., and P.L. Sutherland. 1986. Porosity. In A. Klute (ed.) Methods soil analysis. Part 1. 2nd ed. SSSA Book Ser. 5. ASA and SSSA, Madison, WI.

Harvey, R.W., N.E. Kinner, D. MacDonald, D.W. Metge, and A. Bunn. 1993. Role of physical heterogeneity in the interpretation of small-scale laboratory and field observations of bacteria, microbial-sized microsphere, and bromide transport through aquifer sediments. Water Resour. Res. 29:2713–2721.

Herzig, J.P., D.M. Leclerc, and P. LeGoff. 1970. Flow of suspension through porous media: Application to deep filtration. Ind. Eng. Chem. 62:129–157.

Johnson, P.R., and M. Elimelech. 1995. Dynamics of colloid deposition in porous media: Blocking based on random sequential adsorption. Langmuir 11:801–812.

Kretzschmar, R., M. Borkovec, D. Grolimund, and M. Elimelech. 1999. Mobile subsurface colloids and their role in contaminant transport. Adv. Agron. 66:121–193.

Kretzschmar, R., K. Barmettler, D. Grolimund, Y.-D. Yan, M. Borkovec, and H. Sticher. 1997. Experimental determination of colloid deposition rates and collision efficiencies in natural porous media. Water Resour. Res. 33:1129–1137.

Logan, B.E., D.G. Jewett, R.G. Arnold, E.J. Bouwer, and C.R. O'Melia. 1995. Clarification of clean-bed filtration models. J. Environ. Eng. 121:869–873.

MacCarthy, J.F., and J.M. Zachara. 1989. Subsurface transport of contaminants. Environ. Sci. Technol. 23:496–502.

MacLeod, F.A., H.M. Lappin-Scott, and J.W. Costerton. 1988. Plugging of a model rock system by using starved bacteria. Appl. Environ. Microbiol. 54:1365–1372.

Marquardt, D.W. 1963. An algorithm for least-squares estimation of nonlinear parameters. J. Soc. Indust. Appl. Math. 11:431–441.

Matthess, G., and A. Pekdeger. 1985. Survival and transport of pathogenic bacteria and viruses in groundwater. p. 472–482. In C.H. Ward et al. (ed.) Ground water quality. John Wiley, New York.

McDowell-Boyer, L.M., J.R. Hunt, and N. Sitar. 1986. Particle transport through porous media. Water Resour. Res. 22:1901–1921.

Ouyang, Y., D. Shinde, R.S. Mansell, and W. Harris. 1996. Colloid-enhanced transport of chemicals in subsurface environments: A review. Crit. Rev. Environ. Sci. Technol. 26:189–204.

Pieper, A.P., J.N. Ryan, R.W. Harvey, G.L. Amy, T.H. Illangasekare, and D.W. Metge. 1997. Transport and recovery of bacteriophage PRD1 in a sand and gravel aquifer: Effect of sewage-derived organic matter. Environ. Sci. Technol. 31:1163–1170.

Rajagopalan, R., and C. Tien. 1976. Trajectory analysis of deep-bed filtration with the sphere-in-a-cell porous media model. AIChE J. 22:523–533.

Redman, J.A., S.B. Grant, T.M. Olson, M.E. Hardy, and M.K. Estes. 1997. Filtration of recombinant Norwalk virus particles and bacteriophage MS2 in quartz sand: Importance of electrostatic interactions. Environ. Sci. Technol. 31:3378–3383.

Redman, J.A., S.B. Grant, T.M. Olson, and M.K. Estes. 2001. Pathogen filtration, heterogeneity, and the potable reuse of wastewater. Environ. Sci. Technol. 35:1798–1805.

Reimus, P.W. 1995. The use of synthetic colloids in tracer transport experiments in saturated rock fractures. LA-13004-T. Los Alamos National Laboratory, Los Alamos, NM.

Ryan, J.N., and M. Elimelech. 1996. Colloid mobilization and transport in groundwater. Colloids Surf. A 107:1–56.

Ryan, J.N., M. Elimelech, R.A. Ard, R.W. Harvey, and P.R. Johnson. 1999. Bacteriophage PRD1 and silica colloid transport and recovery in an iron oxide-coated sand aquifer. Environ. Sci. Technol. 33:63–73.

Ryan, J.N., and P.M. Gschwend. 1994. Effect of solution chemistry on clay colloid release from an iron oxide-coated aquifer sand. Environ. Sci. Technol. 28:1717–1726.

Saiers, J.E., G.M. Hornberger, and C. Harvey. 1994. Colloidal silica transport through structured, heterogeneous porous media. J. Hydrol. (Amsterdam) 163:271–288.

Sakthivadivel, R. 1966. Theory and mechanism of filtration of noncolloidal fines through a porous medium. Rep. HEL 15-5. Hydraul. Eng. Lab., Univ. of Calif., Berkeley, CA.

Sakthivadivel, R. 1969. Clogging of a granular porous medium by sediment. Rep. HEL 15-7. Hydraul. Eng. Lab., Univ. of Calif., Berkeley, CA.

Silliman, S.E. 1995. Particle transport through two-dimensional, saturated porous media: Influence of physical structure of the medium. J. Hydrol. (Amsterdam) 167:79–98.

Simunek, J., M. Sejna, and M.Th. van Genuchten. 1999. The HYDRUS-2D software package for simulating two-dimensional movement of water, heat, and multiple solutes in variably saturated media. Version 2.0, IGWMC-TPS-53. International Ground Water Modeling Center, Colorado School of Mines, Golden, CO.

Song, L.F., and M. Elimelech. 1994. Transient deposition of colloidal particles in heterogeneous porous media. J. Colloid Interface Sci. 167:301–313.

Song, L.F., P.R. Johnson, and M. Elimelech. 1994. Kinetics of colloid deposition onto heterogeneously charged surfaces. Environ. Sci. Technol. 28:1164–1171.

Suarez, D.L., J.D. Rhoades, R. Lavado, and C.M. Grieve. 1984. Effect of pH on saturated hydraulic conductivity and soil dispersion. Soil Sci. Soc. Am. J. 48:50–55.

Tan, Y., J.T. Cannon, P. Baveye, and M. Alexander. 1994. Transport of bacteria in an aquifer sand—Experiments and model simulations. Water Resour. Res. 30:3243–3252.

Tufenkji, N., J.A. Redman, and M. Elimelech. 2003. Interpreting deposition patterns of microbial particles in laboratory-scale column experiments. Environ. Sci. Technol. 37:616–623.

Wan, J., T.K. Tokunaga, and C.-F. Tsang. 1995. Bacterial sedimentation through a porous medium. Water Resour. Res. 31:1627–1636.

Wang, D.S., C.P. Gerba, and J.C. Lance. 1981. Effect of soil permeability on virus removal through soil. Appl. Environ. Microbiol. 42:83–88.

Wilson, J.T., L.E. Leach, M. Henson, and J.N. Jones. 1986. In situ biorestoration as a ground water remediation technique. Ground Water Monit. Rev. 6:56–64.

Yao, K., M.T. Habibian, and C.R. O'Melia. 1971. Water and wastewater filtration: Concepts and applications. Environ. Sci. Technol. 5:1105–1112.